X-ray Raman scattering study of $MgSiO_3$ glass at high pressure: Implication for triclustered $MgSiO_3$ melt in Earth's mantle

Sung Keun Lee[a,b], Jung-Fu Lin[b,c], Yong Q. Cai[d], Nozomu Hiraoka[d,e], Peter J. Eng[f,g], Takuo Okuchi[h], Ho-kwang Mao[b,i,j], Yue Meng[i,j], Michael Y. Hu[i], Paul Chow[i], Jinfu Shu[j], Baosheng Li[k], Hiroshi Fukui[l,m], Bum Han Lee[a], Hyun Na Kim[a], and Choong-Shik Yoo[n]

[a]School of Earth and Environmental Sciences, Seoul National University, Seoul, 151-742 Korea; [c]Lawrence Livermore National Laboratory, Livermore, CA 94588; [d]National Synchrotron Radiation Research Center, Hsinchu 30076, Taiwan; [f]Consortium for Advanced Radiation Sources and [g]James Franck Institute, University of Chicago, Chicago, IL 60637; [h]Institute for Advanced Research, Nagoya University, Furo-cho, Chikusa, Nagoya 464-8601, Japan; [i]High Pressure Collaborative Access Team, Advanced Photon Source, Argonne National Laboratory, Argonne, IL 60439; [j]Geophysical Laboratory, Carnegie Institution of Washington, Washington, DC, 20015; [k]Mineral Physics Institute, Stony Brook University, Stony Brook, NY 11794; [l]Institute for Study of the Earth's Interior, Okayama University, Yamada 827, Misasa, Tottori 682-0193, Japan; and [n]Department of Chemistry and Institute for Shock Physics, Washington State University, Pullman, WA 99164

Contributed by Ho-kwang Mao, March 18, 2008 (sent for review January 14, 2008)

Silicate melts at the top of the transition zone and the core-mantle boundary have significant influences on the dynamics and properties of Earth's interior. $MgSiO_3$-rich silicate melts were among the primary components of the magma ocean and thus played essential roles in the chemical differentiation of the early Earth. Diverse macroscopic properties of silicate melts in Earth's interior, such as density, viscosity, and crystal-melt partitioning, depend on their electronic and short-range local structures at high pressures and temperatures. Despite essential roles of silicate melts in many geophysical and geodynamic problems, little is known about their nature under the conditions of Earth's interior, including the densification mechanisms and the atomistic origins of the macroscopic properties at high pressures. Here, we have probed local electronic structures of $MgSiO_3$ glass (as a precursor to Mg-silicate melts), using high-pressure x-ray Raman spectroscopy up to 39 GPa, in which high-pressure oxygen K-edge features suggest the formation of tricluster oxygens (oxygen coordinated with three Si frameworks; $^{[3]}O$) between 12 and 20 GPa. Our results indicate that the densification in $MgSiO_3$ melt is thus likely to be accompanied with the formation of triculster, in addition to a reduction in nonbridging oxygens. The pressure-induced increase in the fraction of oxygen triclusters >20 GPa would result in enhanced density, viscosity, and crystal-melt partitioning, and reduced element diffusivity in the $MgSiO_3$ melt toward deeper part of the Earth's lower mantle.

silicate melts at high pressure | tricluster oxygen

The nature of silicate melts at high pressure and temperature governs magmatic processes in the Earth's interior and it probably dominated the differentiation of Earth in the Hadean magma ocean where significant fractions of the Earth were melts (1–3). It has been suggested that the potential presence of silicate melts, primarily in $MgSiO_3$ composition, at the top of the transition zone (4–6) and in the core-mantle boundary (7, 8) significantly contributes to the seismic heterogeneity of the regions. Pressure-induced structural changes in the silicate melts play an important role in the macroscopic thermodynamic, transport, and electronic properties at high pressure (e.g., refs. 9–13). Despite their importance and implications for global geophysical processes in the Earth's interior as precursors to crystalline $MgSiO_3$ phases, including perovskite and postperovskite (14, 15), the high-pressure structures of $MgSiO_3$ glass and melt remain enigmatic because of their inherent structural disorder and the lack of suitable experimental probes at high pressures. In other binary alkali and ternary aluminosilicate glasses, the densification mechanism is mostly associated with an increase, either gradual or abrupt, in the coordination number of the framework cations, such as Si and Al from 4 to 5 and 6 at the expense of the nonbridging oxygen (NBO) (11, 12, 16–20). However, pressure dependence of the coordination transformation for fully polymerized covalent oxide glasses, including archetypal SiO_2 and B_2O_3 intrinsically results from the formation of the triply coordinated oxygen ($^{[3]}O$), as evidenced from *ab initio* molecular dynamics simulations of the SiO_2 melt at high pressures up to 20 GPa (21) and oxygen K-edge x-ray Raman studies of amorphous B_2O_3 at high pressures (22).

Formation of tricluster is known to be one of the dominant factors affecting the melt properties at high pressure, potentially explaining the anomalous pressure-induced changes in viscosity and oxygen diffusivity (9, 23, 24). The presence of the oxygen tricluster may significantly enhance the partitioning coefficient of an element between crystals and Mg-silicate melts in Earth's interior and probably account for the low solubility of noble gases in the melt at high pressure (25). The formation of five- and sixfolded silicon ($^{[5,6]}Si$) in the highly depolymerized $MgSiO_3$ glass is expected to be associated with the formation of the oxygen tricluster, considering similar densification behavior of Si with the fully polymerized silicates [see the supporting information (SI) for details]; however, experimental evidence for its formation in the silicate melts and glasses at high pressure is lacking. We have recently shown that synchrotron x-ray Raman scattering (also known as inelastic x-ray scattering) with diamond anvil cells (DACs) provides detailed information on the pressure-induced electronic bonding changes for low-z elements in amorphous oxides, such as borates and SiO_2 glasses (22, 26, 27) and other crystalline and molecular compounds (28–32). As discussed in detail in refs. 26 and 28, oxygen K-edge x-ray Raman scattering is currently the only available *in situ* experimental

Author contributions: S.K.L. and J.-F.L. contribute equally to this work; S.K.L., J.-F.L., Y.Q.C., N.H., P.J.E., T.O., H.-k.M., and C.-S.Y. designed research; S.K.L., J.-F.L., Y.Q.C., N.H., P.J.E., T.O., H.-k.M., Y.M., M.H., P.C., J.S., B.L., H.F., B.H.L., and H.N.K. performed research; S.K.L., J.-F.L., Y.Q.C., N.H., P.J.E., H.-k.M., J.S., B.L., and C.-S.Y. contributed new reagents/analytic tools; S.K.L., J.-F.L., Y.Q.C., N.H., P.J.E., H.-k.M., Y.M., M.H., P.C., H.F., B.H.L., and H.N.K. analyzed data; and S.K.L., J.-F.L., Y.Q.C., N.H., P.J.E., T.O., H.-k.M., Y.M., M.H., P.C., and H.F. wrote the paper.

The authors declare no conflict of interest.

Freely available online through the PNAS open access option.

[b]To whom correspondence should be addressed. E-mail: sungklee@snu.ac.kr, lin24@llnl.gov, or h.mao@gl.ciw.edu.

[e]Present address: Brookhaven National Laboratory, Upton, NY 11973.

[m]Present address: SPring8, Hyogo 679-5198, Japan.

This article contains supporting information online at www.pnas.org/cgi/content/full/0802667105/DCSupplemental.

technique to directly reveal the pressure-induced electronic bonding changes around oxygen atoms in oxide glasses. Here, we have studied the oxygen K-edge x-ray Raman spectra of $MgSiO_3$ glass at pressures up to 39 GPa where the formation of the triclustered oxygen bonds at high pressures is suggested.

Results and Discussion

The oxygen K-edge spectra of $MgSiO_3$ glass with a dominant feature at 538–539 eV show negligible changes in the pressure range between 1 atm and ≈12 GPa. Above 20 GPa, the spectra show a distinct feature at ≈544–545 eV, wherein the spectral features gradually shift to higher energies with increasing pressure (Fig. 1 *A* and *B*). The occurrence of the spectral feature near 545 eV at high pressures may stem from a variety of pressure-induced structural changes in the $MgSiO_3$ glass, such as the formation of the $^{[3]}$O tricluster, an increase in the Mg-O distance, reduction in NBO, and formation of oxygen linking $^{[4]}$Si and highly coordinated silicon, such as $^{[4]}$Si–O–$^{[5,6]}$Si and $^{[6]}$Si–O–$^{[6]}$Si.

To explain the spectral feature observed at 544–545 eV in the x-ray Raman spectra of the $MgSiO_3$ glass at high pressure, we explored the oxygen K-edge x-ray Raman spectra for model amorphous and crystalline $MgSiO_3$ and SiO_2 phases at ambient conditions with known short-range local structures [e.g., bridging oxygen (BO), NBO, and edge-sharing oxygen] (Fig. 2). This approach is particularly helpful because the connection between x-ray Raman features and the local oxygen electronic bonding environment has not been fully understood in these materials. The x-ray Raman spectra for amorphous SiO_2 glass at 1 atm and $MgSiO_3$ glass are similar and consist of a broad peak at ≈538 eV, consistent with previous studies of the oxygen K-edge spectra of SiO_2 glasses at 1 atm (27, 33, 34) (Fig. 2*A*). This indicates that both NBO (Mg–O–$^{[4]}$Si) and BO ($^{[4]}$Si–O–$^{[4]}$Si) have similar oxygen K-edge features, arising from the insignificant effect of Mg to the oxygen K-edge feature (Fig. 2*B*). At ≈538 eV, the oxygen K-edge spectrum for quartz shows a distinct feature because of $^{[4]}$Si–O–$^{[4]}$Si (Ref (27, 33, 34).). The spectrum for ilmenite-type $MgSiO_3$ shows distinctive features at 537 and 541 eV. This peculiar feature for the edge-sharing oxygen configuration is similar to that of stishovite (27), indicating close proximity of oxygen around oxygen with its second nearest neighbors. The oxygen K-edge spectrum of pyroxene shows a broad feature at 539–540 eV that stems from the smaller Si–O–Si angles in pyroxene (138.3° and 131.4°) compared with that in quartz (143.6°) (Fig. 2*C*). The oxygen K-edge spectrum of perovskite with all corner-sharing $^{[6]}$Si–O–$^{[6]}$Si shows an increase in the intensity at ≈543 eV (Fig. 1*D*), indicating pressure-induced Si coordination transformation (see SI for more discussion).

The abovementioned analyses of the model systems provide a basis for interpreting the local electronic structures of the $MgSiO_3$ glass at high pressures (Fig. 1). Most of the features relevant to the local oxygen configurations observed for the crystalline phases at high pressure, including both the specific bond angles, length effect of crystals, edge-sharing oxygen (537 and 541 eV), and $^{[6]}$Si–O–$^{[6]}$Si (543 eV), cannot explain the significant changes observed for the glasses at high pressures. In particular, pressure-induced changes in the Mg–O distance or the formation of $^{[4]}$Si–O–$^{[5,6]}$Si because of the reduction in NBO can only partially contribute to the occurrence of the spectral features at 545 eV (Fig. 1*C*). Previous oxygen K-edge studies of B_2O_3 and SiO_2 glasses, using x-ray Raman spectroscopy, have shown that the edge feature is sensitive to the change in the coordination environment of oxygen: Similar features (increase in intensity with pressure in high energy region) were observed for oxygen K-edge x-ray Raman spectra for B_2O_3 glass, which has been attributed to the formation of triply coordinated oxygen with highly coordinated borons, $^{[4]}$B (22). A similar oxygen K-edge feature at 543 eV for SiO_2 glass has been interpreted as the formation of stishovite-like $^{[6]}$Si in SiO_2 glass at high pressures (27). We note that the coordination transformation of Si in the SiO_2 glass is uniquely accompanied by the formation of oxygen atoms that are triply coordinated by $^{[5,6]}$Si. Recent

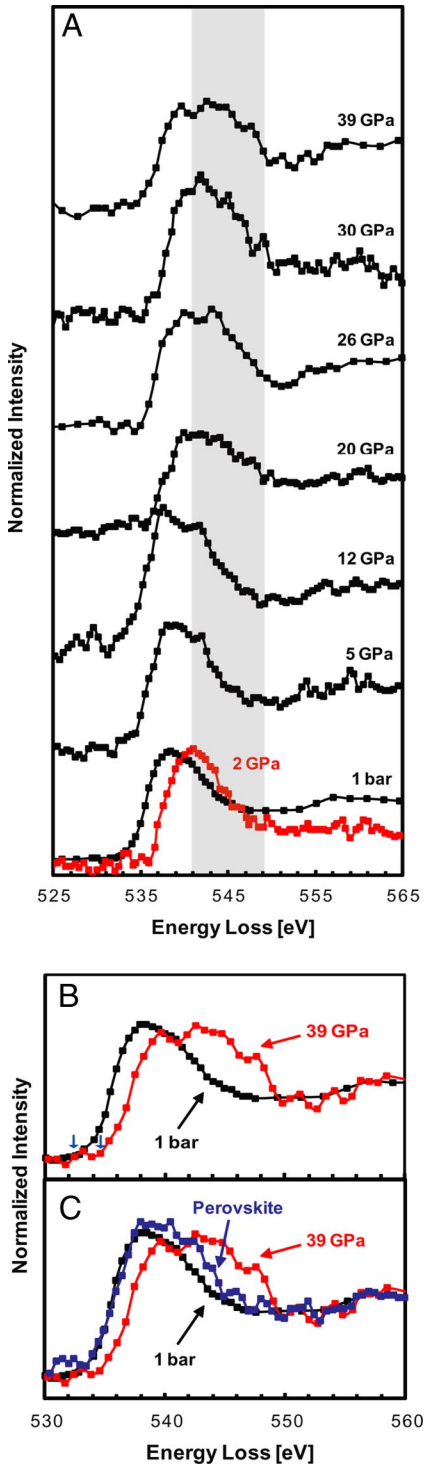

Fig. 1. Oxygen K-edge x-ray Raman spectra for $MgSiO_3$ glasses at high pressures [plotted as energy loss (incident energy − elastic energy) vs. normalized scattered intensity]. (*A*) Total x-ray raman spectra. Gray area represents energy range from 539 to 549 eV. (*B*) Comparison of the Oxygen K-edge spectra for amorphous $MgSiO_3$ at 1 atm and 39 GPa. (*C*) Oxygen K-edge x-ray Raman spectra for $MgSiO_3$ glasses at 1 atm and 39 GPa and perovskite. Points refer to the step size of the energy scan of the experiments (see *Materials and Methods*).

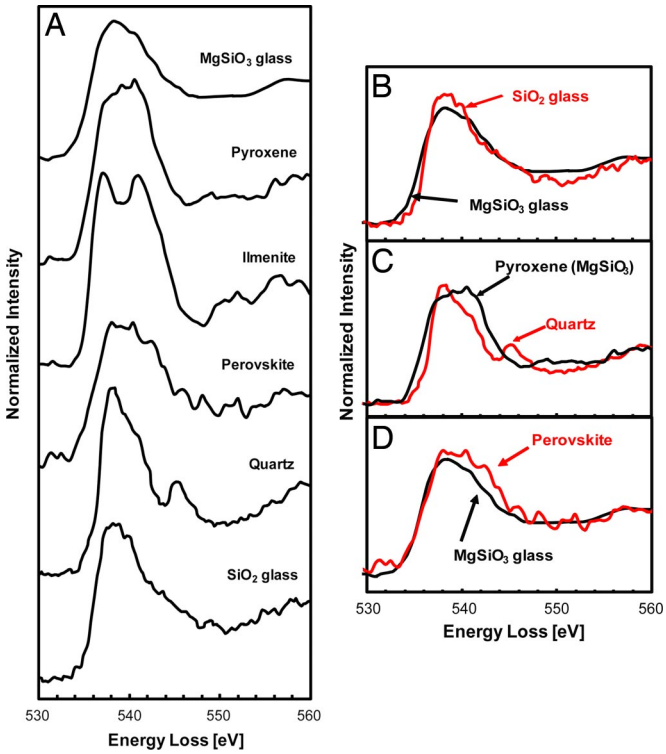

Fig. 2. Oxygen K-edge x-ray Raman spectra for crystalline and amorphous SiO_2 and $MgSiO_3$ at 1 atm and their high-pressure phases. (*A*) Total oxygen K-edge x-ray Raman spectra. (*B*) Oxygen K-edge spectra for amorphous SiO_2 and $MgSiO_3$ at 1 atm. All of the oxygens in the crystalline quartz and amorphous SiO_2 glass at 1 atm are bridging oxygens (BOs) ($^{[4]}$Si–O–$^{[4]}$Si), whereas, in $MgSiO_3$ glass at 1 atm, approximately one-third of the oxygens are BOs, and the rest are nonbridging oxygens (NBOs) (Mg–O–$^{[4]}$Si) (40). The spectral feature in the lower energy region for $MgSiO_3$ glass is slightly broader than that of SiO_2 glass. This can be explained by the existence of the NBO in the former, in which the oxygen 2*p* projected partial density of states has unoccupied states at slightly lower energy than BO (41). The features at 537 and 541 eV in the spectrum for ilmenite-type $MgSiO_3$ are associated with oxygen *p*-*p* hybridization with another nearby oxygen specific for edge-sharing oxygens. (*C*) Oxygen K-edge spectra for pyroxene and quartz. The low energy feature for pyroxene is probably associated with Mg–O–$^{[4]}$Si (41). The 538 eV feature in quartz arises from the transition of the core electrons from 1*s* states to unoccupied oxygen 2*p* states hybridized with the silicon 3*s* and 3*p* states in two nearby $^{[4]}$Si and that at ≈546 eV apparently originates from its long-range periodicity as it becomes prevalent for the larger clusters with several coordination shells in full multiple-scattering simulations (33). (*D*) Oxygen K-edge spectra for amorphous $MgSiO_3$ at 1 atm and perovskite. The significantly different oxygen coordination environments for perovskite and glass at 1atm (i.e., $^{[6]}$Si–O–$^{[6]}$Si for perovskite vs. $^{[4]}$Si–O–$^{[4]}$Si and Mg–O–$^{[4]}$Si for $MgSiO_3$ glass at 1 atm) do not lead to significant changes in the x-ray Raman features.

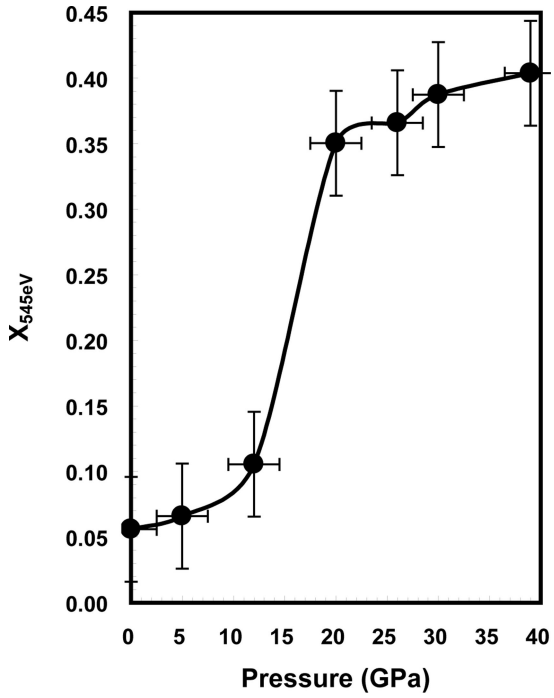

Fig. 3. Pressure dependence of the fraction of the spectral feature centered at 545 eV ($X_{545\ eV}$). The thin solid line is a guide to the eye only. Each spectrum in Fig. 2 was fitted to a model consisting of three Gaussian peaks (one for the 545 eV peak and two for the other regions to obtain relative fraction) and the fraction is obtained by calculating the ratio of the area under the 545 eV peak to the total area from ≈532 eV to 551 eV. As mentioned in the text, the fitting approach is used to provide the qualitative trend in the fractions of the oxygen K-edge features at high pressures.

theoretical calculations of the local structure of SiO_2 glass have shown that a significant increase in the fraction of highly coordinated Si at ≈20 GPa (35), consistent with the changes in the oxygen K-edge x-ray Raman spectra with pressure (27). Molecular dynamics simulations have also reported that the fraction of the oxygen triclusters in $Na_2Si_4O_9$ melt increases from 0% at 1 atm to the 30% at 30 GPa (24). Therefore, the oxygen K-edge feature at 545 eV in the $MgSiO_3$ glass at pressures >20 GPa can be attributed to the formation of the triply coordinated oxygen and changes in the short- to medium-range structures that are associated with the formation of the triply coordinated oxygen at pressures >20 GPa (i.e., formation of a three-member ring, an increase in bond length, and a decrease in bond angle).

The shift in the oxygen K-edge energy of $MgSiO_3$ glass corresponds to the topological changes with pressure, such as the bond length and angle, as reported in refs. 22 and 31. The pressure-induced energy shift in the oxygen K-edge observed here can thus be assigned to ring-statistics associated with a reduction in the bond angle and the formation of smaller member rings. The shift in the edge energy is apparently irreversible when decompressed from >30 GPa. The energy difference of 1–2 eV between the x-ray Raman spectra of the initial and decompressed $MgSiO_3$ glass from 30 GPa to 1 atm cannot be simply explained by the experimental uncertainty in the spectra, because the uncertainty in the energy calibration at the synchrotron beam lines used in this study is <0.4 eV (see SI for details). This irreversible change in edge energy is consistent with the permanent densification of $MgSiO_3$ glass likely due to the changes in the ring-statistics.

To qualitatively understand the fraction of the oxygen tricluster in $MgSiO_3$ glass at high pressures, the ratio of the area under the 545 eV peak to the total area was derived (Fig. 3). Because the feature in the x-ray Raman spectrum can arise from complex multielectronic transitions spanning from pre-edge to the extended region, the Gaussian de-convolution of x-ray Raman spectrum may not properly describe the changes in bonding. The purpose of the current analysis is, therefore, not designed to provide the quantitative information about the fraction of tricluster (the full x-ray Raman profile would be necessary to achieve this feat). Rather, the current fitting approach is used to provide the qualitative trend in the fractions of the oxygen K-edge features that are relevant to the formation of oxygen tricluster at high pressure. A dramatic increase in the fraction of the spectral feature at 545 eV between 12 GPa and 20 GPa in the $MgSiO_3$ glass reveals an electronic bonding transition, which is referred to be due to oxygen coordination transformation. *Ab initio* MD simulations

GEOPHYSICS

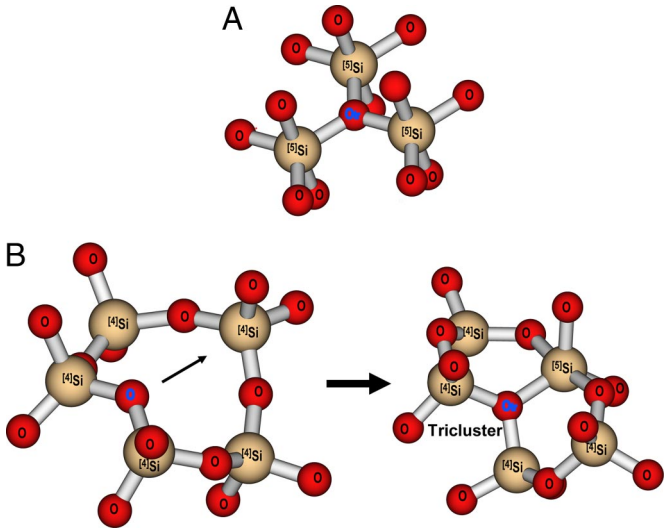

Fig. 4. Structure of oxygen tricluster. (*A*) Schematic local structure of the oxygen tricluster ([3]O, blue oxygen) as one of the examples (see SI for more details). (*B*) Possible mechanism for the formation of the oxygen tricluster. Here, the blue bridging oxygen in the five member ring (*Left*) approaches toward [4]Si and forms [5]Si and tricluster oxygen (*Right*) with three member rings. A similar mechanism for the tricluster formation was proposed for borosilicate glasses at 1 atm (36).

(12, 13) of $MgSiO_3$ liquid at the pressures of the core-mantle boundary indicate that the reduced fraction of the NBO is a major densification mechanism in silicate melts. Together with the formation of the oxygen triclusters, these trends suggest multiple densification mechanisms in the $MgSiO_3$ melt at high pressure. The schematic atomic configuration for one of the oxygen triclusters coordinated with three [5]Si atoms responsible for the high-energy edge feature (Fig. 4*A*) is shown along with a possible mechanism of its formation (Fig. 4*B*). Although the mechanism is based on the transformation of the BO to [3]O with pressure, it is likely that the oxygen triclusters in $MgSiO_3$ glasses can also be formed from the NBO (NBO $\rightarrow$ [3]O). The formation of the triclusters in Mg-silicates may initiate the formation of smaller member rings (including three-member rings), in which the larger member ring (e.g., a five-member ring) acts as a strain energy reservoir in the formation of the highly coordinated Si and tricluster (Fig. 4*B*) (36). The broadening of the oxygen K-edge feature in $MgSiO_3$ glass also suggests an increase in the topological disorder and significant changes in the medium-range order with increasing pressures (37), although the detailed atomic configurations and effects on the x-ray Raman features require further exploration.

Our study of $MgSiO_3$ glass—a precursor for the $MgSiO_3$ melt at high pressures—indicates the formation of the oxygen triclusters and associated changes in the atomic configuration in short-to-medium range, with a reduction in the NBO, above $\approx$20 GPa. These changes would affect the thermodynamic (e.g., density, molar volume, and crystal-melt partitioning) and transport properties of silicate melts (e.g., viscosity and diffusivity) toward the deeper part of the Earth's lower mantle. Although the effect of temperature needs further exploration to obtain insights into melts, the formation of oxygen triclusters can be an efficient densification mechanism in the $MgSiO_3$ melt in Earth's mantle and may explain the atomistic origin of the high-density Mg-silicate melts at the core-mantle boundary (7, 8). Changes in the local electronic structure and composition of silicate melts are believed to promote the partitioning of elements between crystalline phases and melts in the Earth's mantle (10, 38, 39). The increase in the fraction of the oxygen triclusters with smaller member rings results in a reduced free volume needed to host elements that are more incompatible. That is, the triclustered oxygens increase the crystal-melt partitioning coefficient ($D^{\text{crystal-melt}}$) of elements, such as radioactive nuclides [i.e., $(d^{[3]}O/dP)_T = (dD^{\text{crystal-melt}}/dP)_T$], thereby significantly affecting the process of the chemical differentiation in the Hadean magma oceans. The continuous increase in the fraction of the triclustered $MgSiO_3$ melt at high pressures and temperatures thus needs to be taken into account in future modeling to improve our understanding of the microscopic origins of the geochemical and geophysical processes in the Earth's interior.

Materials and Methods

$MgSiO_3$ glass was synthesized by melting $MgCO_3$ and SiO_2 powder at 1,650°C and quenching to ambient conditions. The samples were loaded into the sample chamber of a Be gasket in a DAC with a few ruby spheres as the pressure calibrant without a pressure medium. Because no pressure medium was used to minize scattering or absorption from pressure medium, the stress condition upon pressurization in DAC is uniaxial. Although stress conditions upon compression (i.e., uniaxial vs. hydrostatic) may affect the glass structure under pressure, its effect is unlikely to be significant, mostly because of the isotropic nature of the silicate glasses without directional bonding changes with pressure. An experiment with hydrostatic condition (with the pressure medium) is essential to explore the effect of stress condition on the pressure-induced changes in electroning bonding environment in oxide glasses including borate that apparently have directional bonding associated with boroxol ring. Diamonds with flat culets of 150–500 μm depending on the phases and pressure ranges of the experiments were used for high-pressure x-ray Raman experiments up to 39 GPa. The thickness of the sample in the gasket was $\approx$30–80 μm at high pressures. Crystalline $MgSiO_3$ pyroxene was synthesized in a gas-mixing furnace, and ilmenite and perovskite samples were synthesized in a multianvil apparatus. It should be mentioned that the crystal structures of these materials were confirmed by x-ray diffraction and optical Raman spectroscopy before experiments.

The x-ray Raman spectra were collected at beam line BL12-XU of the SPring-8 (for crystalline $MgSiO_3$ phases and $MgSiO_3$ glass at 1 bar and 5 GPa, respectively), beam line 13ID-C of the Geo Soil Enviro Consortium for Advanced Radiation Sources (1 bar, 26 GPa, and 39 GPa), and beam line 16ID-C of the High Pressure Collaborative Access Team (at 12, 20, 30, and 2 GPa for decompressed $MgSiO_3$ glass from 30 GPa, quartz, and SiO_2 glass) of the Advanced Photon Source. X-ray Raman spectra for these crystalline samples and SiO_2 glass at 1 bar were collected for the samples mounted directly on the goniometer without DAC (and thus without cold compression). The x-ray Raman spectra were collected by scanning the energy of the incident beam relative to the analyzer with a fixed elastic energy (E_0) of 9.886 keV at beam line BL12XU, 9.692 keV at the Geo Soil Enviro Consortium for Advanced Radiation Sources, and 9.686 keV at the High Pressure Collaborative Access Team. The x-ray Raman scattering signals were collected at a scattering angle of 18° at the Geo Soil Enviro Consortium for Advanced Radiation Sources and 30° at the High Pressure Collaborative Access Team with a linear array of six spherical Si (660) analyzers operating in a backscattering geometry. An array of three Si (555) analyzers with a scattering angle of 30° were used for the experiment performed at BL12-XU (31). Oxygen K-edge spectra were collected at pressures up to 39 GPa. A two-point smoothing was used. The x-ray beam size was $\approx$80 μm horizontally and 20 μm vertically at the Geo Soil Enviro Consortium for Advanced Radiation Sources and High Pressure Collaborative Access Team and was 20 $\times$ 20 μm at the BL12-XU. X-ray Raman spectra were collected with $\approx$0.5 eV steps for the data collected at the High Pressure Collaborative Access Team and BL12-XU. At the Geo Soil Enviro Consortium for Advanced Radiation Sources, the x-ray Raman spectrum near the main edge feature was scanned at an energy step of $\approx$0.7 eV from 532 to 550 eV; scan steps of 1.9 eV and 1 eV were used for data collection $>$550 eV and $<$532 eV, respectively. No significant spectral feature was observed from $\approx$522 to 532 eV, which was used as the background spectrum. Raw x-ray Raman spectra were background-subtracted, and then most of the spectra were normalized to the continuum energy tail $>$555 eV. By comparing the spectra from the three beam lines used, the uncertainty in the edge energy of the spectra was identified to be $<$0.4 eV (see SI for details). The pressure uncertainties were calculated from multiple measurements from the ruby spheres before

and after the x-ray measurements, which can be attributed to the relaxation of the sample chamber during the experiments and the pressure gradient across the sample.

ACKNOWLEDGMENTS. We thank I. Jarrige, H. Ishii, V. Iota-Herbei, A. Lazicki, and N. Ito for their assistance in the high-pressure XRS experiments; J. Kung (National Cheng-Kung University, Tainan, Taiwan) for the $MgSiO_3$ glass sample to J.F.L, and T. Yamanaka (Osaka University, Osaka, Japan) for the ilmenite sample. We thank Professor E. Ohtani and Dr. C. Kao for careful and constructive suggestions and advice. We also thank M. Newville for helpful discussion on theoretical calculations of x-ray Raman spectra. Use of the Advanced Photon Source was supported by Department of Energy Basic Energy Sciences under Contract W-31-109-Eng-38. The Geo Soil Enviro Consortium for Advanced Radiation Sources was supported by Department of Energy-Basic Energy Sciences-Geosciences, National Science Foundation Earth Sciences and the State of Illinois. The High Pressure Collaborative Access Team was supported by Department of Energy Basic Energy Sciences Materials Science, the Department of Energy National Nuclear Security Administration, the Carnegie/Department of Energy Alliance Center, the National Science Foundation, and the W. M. Keck Foundation. Experiments performed at beam line BL12-XU of SPring-8 were partly supported by the National Synchrotron Radiation Research Center and National Science Council of Taiwan. This work at Lawrence Livermore National Laboratory was performed under the auspices of the U.S. Department of Energy by the University of California/Lawrence Livermore National Laboratory under Contract W-7405-Eng-48. This work was supported by the Korea Science and Engineering Foundation Grant 2007-000-20120-0 (to S.K.L.) through the National Research Laboratory Program, a Lawrence Livermore Fellowship (to J.F.L.), and the 21st century Center of Excellence program of the Institute for Study of the Earth's Interior (H.F.).

1. Tonks WB, Melosh HJ (1993) Magma ocean formation due to giant impacts. *J Geophy Res Planet* 98:5319–5333.
2. Ohtani E (1985) The primordial terrestrial magma ocean and its implication for stratification of the mantle. *Phys Earth Planet Int* 38:70–80.
3. Labrosse S, Hernlund JW, Coltice N (2007) A crystallizing dense magma ocean at the base of the Earth's mantle. *Nature* 450:866–869.
4. Revenaugh J, Sipkin SA (1994) Seismic evidence for silicate melt atop the 410 Km mantle discontinuity. *Nature* 369:474–476.
5. Sakamaki T, Suzuki A, Ohtani E (2006) Stability of hydrous melt at the base of the Earth's upper mantle. *Nature* 439:192–194.
6. Song TRA, Helmberger DV, Grand SP (2004) Low-velocity zone atop the 410-km seismic discontinuity in the northwestern United States. *Nature* 427:530–533.
7. Akins JA, Luo SN, Asimow PD, Ahrens TJ (2004) Shock-induced melting of $MgSiO_3$ perovskite and implications for melts in Earth's lowermost mantle. *Geophys Res Lett* 31:L14612.
8. Williams Q, Garnero EJ (1996) Seismic evidence for partial melt at the base of Earth's mantle. *Science* 273:1528–1530.
9. Angell CA, Cheeseman PA, Tamaddon S (1982) Pressure enhancement of ion mobilities in liquid silicates from computer simulations studies to 800 kbar. *Science* 218:885–887.
10. Lee SK, Cody GD, Fei Y, Mysen BO (2004) The nature of polymerization and properties of silicate glasses and melts at high pressure. *Geochim Cosmochim Acta* 68:4189–4200.
11. Yarger JL, *et al.* (1995) Al coordination changes in high-pressure aluminosilicate liquids. *Science* 270:1964–1967.
12. Stixrude L, Karki B (2005) Structure and freezing of $MgSiO_3$ liquid in Earth's lower mantle. *Science* 310:297–299.
13. Laudernet Y, Clerouin J, Mazevet S (2004) Ab initio simulations of the electrical and optical properties of shock-compressed SiO_2. *Phys Rev B* 70:165108.
14. Oganov AR, Ono S (2004) Theoretical and experimental evidence for a post-perovskite phase of $MgSiO_3$ in Earth's D'' layer. *Nature* 430:445–448.
15. Murakami M, Hirose K, Kawamura K, Sata N, Ohishi Y (2004) Post-perovskite phase transition in $MgSiO_3$. *Science* 304:855–858.
16. Wolf GH, McMillan PF (1995) in *Structure, Dynamics, and Properties of Silicate Melts*, eds Stebbins JF, McMillan PF, Dingwell DB (Mineralogical Society of America, Washington, DC), Vol 32, pp 505–562.
17. Xue X, Stebbins JF, Kanzaki M, Tronnes RG (1989) Silicon coordination and speciation changes in a silicate liquid at high pressures. *Science* 245:962–964.
18. Allwardt JR, *et al.* (2005) Aluminum coordination and the densification of high-pressure aluminosilicate glasses *Am Mineral* 90:1218–1222.
19. Lee SK, Fei Y, Cody GD, Mysen BO (2003) Order and disorder of sodium silicate glasses and melts at 10 GPa. *Geophys Res Lett* 30:1845.
20. Xue X, Stebbins JF, Kanzaki M (1994) Correlations between O-17 NMR parameters and local structure around oxygen in high-pressure silicates and the structure of silicate melts at high pressure. *Am Mineral* 79:31–42.
21. Trave A, Tangney P, Scandolo S, Pasquarello A, Car R (2002) Pressure-induced structural changes in liquid SiO_2 from ab initio simulations. *Phys Rev Lett* 89:245504.
22. Lee SK, *et al.* (2005) Probing of bonding changes in B_2O_3 glasses at high pressure with inelastic x-ray scattering. *Nat Mater* 4:851–854.
23. Stebbins JF, Xu Z (1997) NMR evidence for excess non-bridging oxygen in aluminosilicate glass. *Nature* 390:60–62.
24. Diefenbacher J, McMillan PF, Wolf GH (1998) Molecular dynamics simulations of $Na_2Si_4O_9$ liquid at high pressure. *J Phys Chem B* 102:3003–3008.
25. Bouhifd MA, Jephcoat AP (2006) Aluminium control of argon solubility in silicate melts under pressure. *Nature* 439:961–964.
26. Lee SK, Eng PJ, Mao HK, Meng Y, Shu JF (2007) Structure of alkali borate glasses at high pressure. *Phys Rev Lett* 98:105502.
27. Lin JF, *et al.* (2007) Electronic bonding transition in compressed SiO_2 glass. *Phys Rev B* 75:012201.
28. Cai YQ, *et al.* (2005) Ordering of hydrogen bonds in high-pressure low-temperature H_2O. *Phys Rev Lett* 94:025502.
29. Wernet P, *et al.* (2004) The structure of the first coordination shell in liquid water. *Science* 304:995–999.
30. Meng Y, *et al.* (2004) The formation of sp(3) bonding in compressed BN. *Nat Mater* 3:111–114.
31. Mao WL, *et al.* (2003) Bonding changes in compressed superhard graphite. *Science* 302:425–427.
32. Bergmann U, *et al.* (2002) X-ray Raman spectroscopy at the oxygen K edge of water and ice: Implications on local structure models. *Phys Rev B* 66:092107.
33. Davoli I, *et al.* (1992) Structure of densified vitreous silica - silicon and oxygen Xanes spectra and multiple-scattering calculations. *Phys Chem Mineral* 19:171–175.
34. Wu ZY, Seifert F, Poe B, Sharp T (1996) Multiple-scattering calculations for SiO_2 polymorphs: A comparison to ELNES and XANES spectra. *J Phys Cond Matt* 8:3323–3336.
35. Liang YF, Miranda CR, Scandolo S (2007) Mechanical strength and coordination defects in compressed silica glass: Molecular dynamics simulations. *Phys Rev B* 75:024205.
36. Lee SK, Musgrave CB, Zhao P, Stebbins JF (2001) Topological disorder and reactivity of borosilicate glasses: Ab initio molecular orbital calculations and ^{17}O and ^{11}B NMR. *J Phys Chem B* 105:12583–12595.
37. Inamura Y, Katayama Y, Utsumi W, Funakoshi K (2004) Transformations in the intermediate-range structure of SiO_2 glass under high pressure and temperature. *Phys Rev Lett* 93:015501.
38. Corgne A, Liebske C, Wood BJ, Rubie DC, Frost DJ (2005) Silicate perovskite-melt partitioning of trace elements and geochemical signature of a deep perovskitic reservoir. *Geochim Cosmochim Acta* 69:485–496.
39. Murthy VR, van Westrenen W, Fei Y (2003) Experimental evidence that potassium is a substantial radioactive heat source in planetary cores. *Nature* 423:163–165.
40. Lee SK, Mysen BO, Cody GD (2003) Chemical order in mixed cation silicate glasses and melts. *Phys Rev B* 68:214206.
41. Jiang N, Denlinger JD, Spence JCH (2003) Electronic structure and oxygen bonding in $CaSiO_3$ silicate. *J Phys Cond Matt* 15:5523–5533.